Real-Space Observation of Drift States in a Two-Dimensional Electron System at High Magnetic Fields

M. Morgenstern, J. Klijn, Chr. Meyer, and R. Wiesendanger

Institute of Applied Physics, Hamburg University, Jungiusstraße 11, D-20355 Hamburg, Germany

(Received 25 September 2002; published 6 February 2003)

The local density of states of the adsorbate-induced two-dimensional electron system is studied in magnetic fields up to $B = 6$ T. Landau quantization is observed and drift states with a width of about the magnetic length are found in agreement with theoretical predictions. At the tails of the Landau levels the states form closed paths indicating localization. These states show the expected energy dependence. A multifractal analysis applied to the data results in a nice parabolic shape of the characteristic $f(\alpha)$ spectra, but we find only a slight displacement of the origin from $\alpha = 2.0$ for the states in the center of the Landau level.

DOI: 10.1103/PhysRevLett.90.056804 PACS numbers: 73.21.Fg, 68.37.Ef, 73.43.Fj, 73.43.Jn

The discovery of the quantum Hall effect in 1980 [1] triggered a wealth of work on the electronic properties of two-dimensional electron systems (2DESs), which have been described as a gold mine of new physics [2]. The quantum Hall effect itself is considered as a consequence of the localized character of wave functions at all energies except in the center of a Landau level (LL), where a single extended state exists [3]. A microscopic description of localized and extended states has been given by Joynt *et al.*, who concluded that noninteracting electrons in a static disorder potential exhibit so-called drift states, which run along equipotential lines of the disorder and exhibit a width of about the magnetic length l_B [4]. The properties of these states have been intensively studied by theory with respect to the energy dependence of the localization length and the multifractal properties of the extended states [5]. Transport experiments, which indirectly probe the energy dependence of the localization length, are in reasonable agreement with the theoretical predictions [6]. However, the drift states themselves have never been probed on the appropriate length scale, i.e., l_B.

Here, we use the adsorbate-induced 2DES, previously studied at $B = 0$ T [7] to probe the drift states by scanning tunneling spectroscopy (STS). The adsorbate-induced 2DES provides the advantage that it is located close to the surface leading to high lateral resolution. Moreover, it is prepared *in situ* by Fe adsorption on the cleavage plane of InAs, which avoids any influence of contamination and surface defects on the electronic properties of the 2DES [8]. Indeed, the 2DES disorder potential $V(x, y)$ exhibits a disorder strength of only $\sigma(V) \simeq 5$ meV [7]. This is larger than in very high mobility 2DESs, but considerably smaller than the Landau quantization energy of 30 meV at $B = 6$ T, which ensures that drift states of different LLs are energetically separated. Moreover, the magnetic length of 10.5 nm at $B = 6$ T is smaller than the correlation length of $V(x, y)$ of 30 nm being the necessary condition for the existence of drift states. The relatively strong disorder with respect to high mobility 2DESs is also an advantage, since at lower disorder electron-electron interactions can guide the system and may prohibit the observation of drift states [9].

The UHV low-temperature scanning tunneling microscope is described in [10]. It works at $T = 6$ K and in magnetic fields up to $B = 6$ T perpendicular to the sample surface. Degenerate n-InAs ($N_D = 1.1 \times 10^{16}/\mathrm{cm}^3$) is cleaved *in situ* at a base pressure below 1×10^{-8} Pa. This results in a clean InAs(110) surface with an adsorbate density of $10^{-7}/\text{Å}^2$, an even lower surface vacancy density, and a step density below $0.1/\mu$m. To induce the 2DES, Fe is deposited on the surface from an e-beam evaporator [11]. The Fe coverage is determined by counting the Fe atoms and is given with respect to the unit cell of InAs(110). The Fe atoms mainly form monomers on the surface acting as surface donors. The resulting band bending and the subband energies of the 2DES are measured by angle-resolved ultraviolet photoemission (ARUPS) with an accuracy of about 5 meV [7,11].

For STS, we use an *ex situ* etched and *in situ* prepared W tip. The local differential conductivity $dI/dV(V, x, y)$ is recorded by lock-in technique ($f = 1.5$ kHz, $V_{\mathrm{mod}} = 0.4$–3 $\mathrm{mV_{rms}}$) with the tip-surface distance fixed at current I_{stab} and voltage V_{stab}. Maps of the local density of states (LDOS) result from (x, y) arrays of dI/dV at constant V [12]. Potential maps are recorded by using the position dependence of the lowest state energy of the tip-induced quantum dot (QD) [7,13]. Such maps represent the screened disorder potential of the 2DES. Several tests are performed to check that the tip has not changed during a set of measurements. In particular, characteristic dI/dV curves and the atomic resolution images are compared prior and after a set of measurements.

Figure 1 shows two sets of spatially averaged dI/dV curves obtained on different samples at slightly different coverage. The subband energies determined from ARUPS are indicated as E_n. A QD state results in a peak at energies below E_0 [7,8], which is visible only in

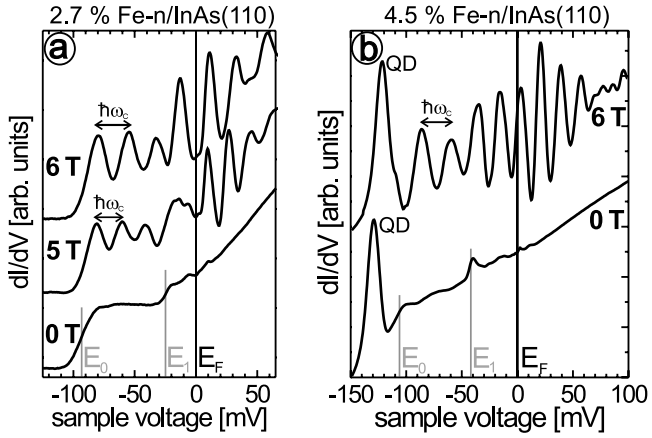

FIG. 1. dI/dV curves spatially averaged over 100×100 nm^2: (a) 2.7% Fe/n-InAs(110), $V_{\text{stab}} = 100$ mV, $I_{\text{stab}} = 300$ pA, $V_{\text{mod}} = 1.8$ mV; different B fields, subband energies E_0, E_1, Fermi level E_F, and expected Landau level splittings $\hbar\omega_c$ are indicated; (b) 4.5% Fe/n-InAs(110), $V_{\text{stab}} = 100$ mV, $I_{\text{stab}} = 500$ pA, $V_{\text{mod}} = 2$ mV; labels as in (a); QD marks the peak corresponding to the tip induced quantum dot [13].

Fig. 1(b). Thus, a QD is present only in the measurements of Fig. 1(b). Steplike structures are found in both figures at the corresponding E_n ($B = 0$ T). This indicates the steplike DOS of a 2DES as discussed in Ref. [7]. At higher B field, regularly separated peaks are found in the area of the 2DES. The peak separation corresponds to the LL separation $\hbar\omega_c = \hbar eB/m_{\text{eff}}$ (m_{eff}: effective mass of InAs). Since m_{eff} increases with energy, the LL separation slightly decreases with energy [14]. Moreover, the LL separation scales with B as expected [15]. Note that the lowest LL peak energy depends on the actual filling factor. The fact that the peaks are observable in the presence and the absence of the QD peak reveals that they are caused by the 2DES [16]. Interestingly, the peak widths are smaller in the second subband, which is in accordance with the known decreasing influence of the disorder on higher subbands [17]. Finally, a beating of the LLs is visible, in particular, in Fig. 1(b). It might be due to the overlap of different subbands with different $m_{\text{eff}}(E)$ or due to the Rashba splitting [18].

Figures 2(a)–2(d) show spatial maps of dI/dV at different V. Figure 2(e) shows the corresponding spatially averaged $dI/dV(V)$ curve, and Fig. 2(f) shows the according disorder potential measured with the help of the QD peak [7,19]. The dI/dV maps exhibit stripelike structures elongated irregularly across the probed area. The width of these structures is close to l_B. To demonstrate that, we took line sections across the stripes and determined the full width at half maximum (FWHM). A histogram of the FWHM is shown in Fig. 2(g) and indeed exhibits a width distribution around $l_B = 10.5$ nm. The corruption strength in the dI/dV images is 75% ± 5% [20], a value which is larger than for the same 2DES at $B = 0$ T (60% ± 5%) [7], much larger than for a similar 3DES at $B = 0$ T (3% ± 0.5%) [21] and also larger than for the 3DES in the extreme quantum limit (30%–65%) [22]. Thus, we observe rather strong LDOS corrugations indicating strongly fluctuating wave functions.

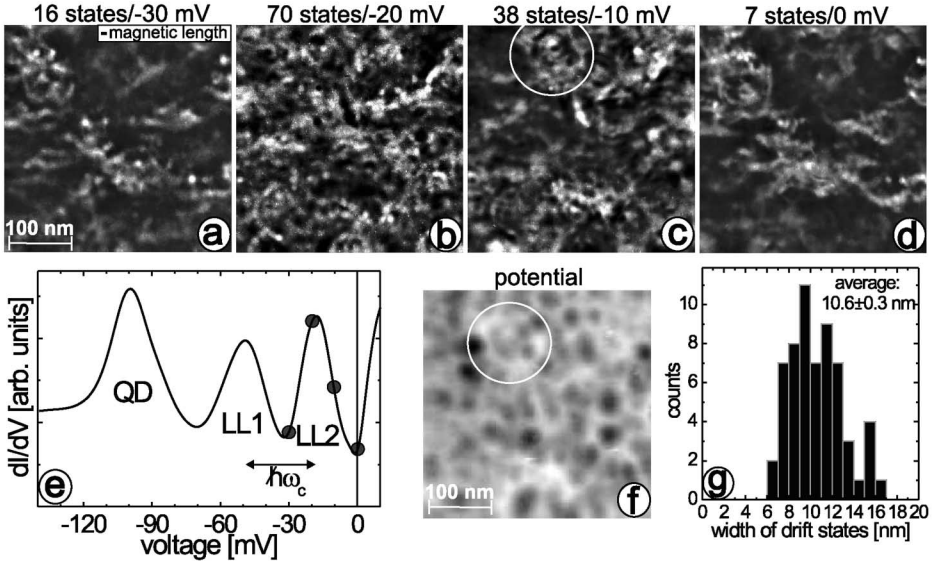

FIG. 2. (a)–(d) dI/dV images of 0.8% Fe/n-InAs(110) recorded at different V as indicated, $B = 6$ T, $V_{\text{stab}} = 100$ mV, $I_{\text{stab}} = 300$ pA, $V_{\text{mod}} = 1.8$ mV; the average number of contributing states $\overline{N}$ is given above each image; (e) spatially averaged dI/dV curve, $V_{\text{stab}} = 100$ mV, $I_{\text{stab}} = 300$ pA, $V_{\text{mod}} = 1$ mV; quantum dot peak (QD), Landau level (LLn), and Landau energy $\hbar\omega_c$ are indicated; dots mark the voltages corresponding to the images (a)–(d); (f) disorder potential of measured area determined with the help of the QD [7]; (g) histogram of determined FWHM of drift states. White rings mark the same area in (c) and (f).

We find that some of the stripe structures are nearly identical to structures in the disorder potential. An example is enclosed by the white rings in Figs. 2(c) and 2(f). Here, the state obviously drifts along a ridge of the potential landscape. Other similarities between potential and LDOS can be found in the images. Note that similarities can also be observed between the two LDOS maps in Figs. 2(a) and 2(d). This is due to the fact that both images are obtained at similar energy distance from a LL peak center, albeit from a different one. Thus, the states drift along a similar part of the potential landscape, although slightly different interactions of different LLs with the disorder potential lead to slightly different images.

A particularly interesting property of drift states is their energy dependence. Since they probe equipotential lines, patterns at adjacent energies should probe adjacent equipotential lines. More precisely, energetically consecutive states localized at the same potential feature should probe rather close equipotential lines. This can indeed be seen in Fig. 3, where four features are followed up over a small energy range. The energies are chosen to be in the tail of the LLs, where a distinction of different patterns is possible (see Fig. 2). One sees that Figs. 3(a)–3(f) and Figs. 3(g)–3(j) show two structures opening up with decreasing energy, Figs. 3(k)–3(n) exhibit an upper structure getting smaller and a lower structure getting larger, and Figs. 3(o)–3(r) show a structure closing down. All structures basically exhibit closed loops indicating that they correspond to localized states. Note that the structures in Figs. 3(a)–3(j) measured at 2.7% coverage are slightly larger than the structures in Figs. 3(k)–3(r), which coincides with the previously noted fact that the potential gets smoother, respectively, gets a larger correlation length, with increasing coverage [7]. A closer inspection of the images gives the impression that the structures are not moving continuously, but consist of two structures contributing with different intensity to images at different energy. The latter is physically expected, since the closed cycle performed by the drift state results in a quantization condition, i.e., the path length must coincide with a multiple of the cyclotron diameter.

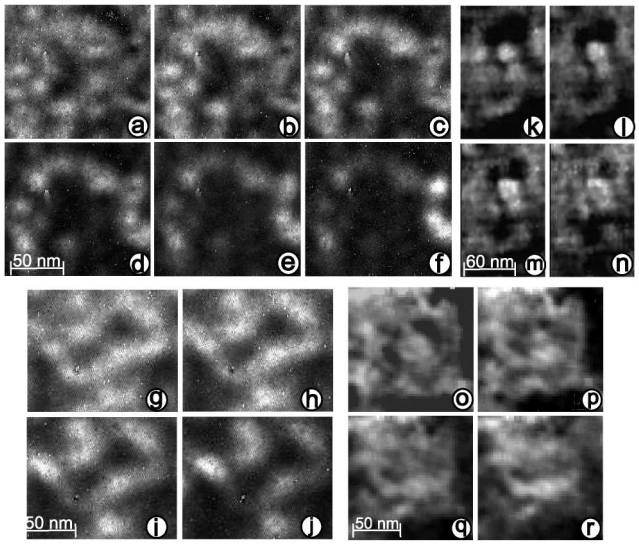

FIG. 3. dI/dV images at $B = 6$ T: (a)–(j) 2.7% Fe, $V_{\text{stab}} = 100$ mV, $I_{\text{stab}} = 300$ pA, $V_{\text{mod}} = 1.8$ mV; (k)–(r) 0.8% Fe, $V_{\text{stab}} = 100$ mV, $I_{\text{stab}} = 300$ pA, $V_{\text{mod}} = 1$ mV; sets in (a)–(f), (g)–(j), (k)–(n), and (o)–(r) show the same area, respectively; (a) $V = -82.6$ mV, (b) $V = -85.6$ mV, (c) $V = -88.6$ mV, (d) $V = -91.6$ mV, (e) $V = -94.6$ mV, (f) $V = -97.6$ mV; (g) $V = -82.6$ mV; (h) $V = -85.6$ mV, (i) $V = -88.6$ mV, (j) $V = -91.6$ mV; (k) $V = -26.9$ mV; (l) $V = -24.5$ mV, (m) $V = -23.4$ mV, (n) $V = -21.6$ mV; (o) $V = -0.5$ mV, (p) $V = -2.9$ mV, (q) $V = -5.7$ mV, (r) $V = -7.6$ mV; bright spikes in the images are Fe atoms.

In the center of the LL [Fig. 2(b)], where the stripelike appearance of the LDOS is still evident, one cannot follow up the development of particular lines across the sample. The reason is simply that the density of states (DOS) increases strongly towards the center of the LL. The average number of states contributing to the LDOS, $\overline{N} = \text{DOS} \times A \times \Delta E$ (A: image area; ΔE: energy resolution), is $\overline{N} \simeq 70$ in Fig. 2(b). On the other hand, the localization length diverges close to the center of the LL according to $|E - E_{\text{LL}}|^{-2.35}$ [5]. Consequently, the space available for a single state, 50×50 nm^2, is smaller than its localization length prohibiting the identification of individual states. In particular, the expected extended state cannot be probed individually [23].

Nevertheless, we applied the multifractal analysis, until now exclusively used to analyze theoretical data [5]. We calculated the qth moment of the measured LDOS and divided the resulting images into boxes of length δ in order to determine the fractal dimension of the image $\alpha(q)$. In a similar way, we determined the corresponding Haussdorf dimension of the images $f(q)$ as described in

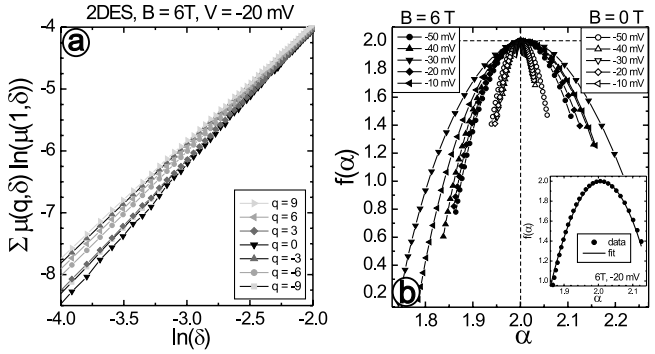

FIG. 4. (a) $\sum_i \mu_i(q, \delta) \ln[\mu_i(1, \delta)]$ versus $\ln(\delta)$ at different q for the data of Fig. 2(b) (see text); (b) $f(\alpha)$ spectra for the data set shown in Fig. 2 ($B = 6$ T) and for a data set from the same 2DES at $B = 0$ T [Figs. 2(i)–2(k) of [7]]; inset: $f(\alpha)$ for $B = 6$ T, $V = -20$ mV (points) and parabolic fit (line).

[24]. Figure 4(a) reveals the required largely linear slope of $\sum_i \mu_i(q, \delta) \ln[\mu_i(1, \delta)]$ versus $\ln(\delta)$, where $\mu_i(\delta, q)$ is the integral of the qth moment of the LDOS over the box at position i. The resulting slope towards small δ is the fractal dimension $\alpha(q)$, e.g., $\alpha(1)$ is the dimension of the LDOS pattern. The $f(q)$ data are determined analogously by simply replacing the 1 in the sum formula by a q. The resulting $f(\alpha)$ spectra are considered to be characteristic of the corresponding quantum phase, respectively, the quantum phase transition in the center of a LL. They are shown in Fig. 4(b) for $B = 6$ T and $B = 0$ T (data from Ref. [7]). The spectra are largely parabolic as evidenced for the LDOS in the center of the Landau level (inset). Note that the $f(\alpha)$ spectra at $B = 0$ T are smaller than at $B = 6$ T. This coincides with the fact that the corrugation at $B = 0$ T is smaller and the patterns are less irregular. A tendency of broadening with decreasing energy at $B = 0$ T reflects the stronger tendency for localization at lower energy. At $B = 6$ T, the broadest spectra are found in the tails of the LL, which we interpret as a result of the better separation of individual states in the tail [25].

Importantly, the origin of the parabola is always close to $\alpha \simeq 2.0$. Even in the center of the LL, it is not at $\alpha = 2.35$ as expected for the extended state and characteristic for the metal-insulator transition in the quantum Hall regime [5]. It is at $\alpha = 2.01 \pm 0.002$. The reason for this discrepancy is found straightforwardly by comparison with numerical data [26]. They show that the parabola is shifted towards $\alpha = 2.0$ by adding up a number of localized states to the extended one [26]. Thus, the identification of the specific multifractal spectrum of the extended state has to be postponed to measurements with lower ΔE, i.e., at lower T [23]. However, the linearity of the curves as shown in Fig. 4(a) and the nice parabolic shape of the resulting $f(\alpha)$ spectra demonstrate that the multifractal analysis can also be applied successfully to experimental data.

In summary, we presented the first experimental observation of drift states appearing in a two-dimensional electron system in high magnetic fields. In agreement with theoretical predictions, the width of the drift states is found to be close to the magnetic length and the states are elongated along equipotential lines of the static disorder potential. Individual states are identified at the tails of the LL, but not in the center where the extended state is proposed to exist. A multifractal analysis of the LDOS data reveals a nice parabolic shape of the $f(\alpha)$ spectra with an origin close to $\alpha = 2.0$. The latter deviates from the expected origin of the extended state, which is due to the contribution of several states to the LDOS data.

We thank R. A. Römer, V. Uski, and E. Schweitzer for helpful discussions. Financial support from Wi 1277/15-2 and Graduiertenkollegs "Physik nanostrukturierter Festkörper," "Spektroskopie an lokalisierten, atomaren Systeme" of the DFG is gratefully acknowledged.

[1] K. v. Klitzing *et al.*, Phys. Rev. Lett. **45**, 494 (1980).
[2] F. Perrot *et al.*, Phys. Rev. Lett. **87**, 206404 (2001).
[3] R. E. Prange *et al.*, *The Quantum Hall Effect* (Springer, New York, 1987).
[4] R. Joynt *et al.*, Phys. Rev. B **29**, 3303 (1984).
[5] See, e.g., M. Y. Azbel *et al.*, Philos. Mag. B **50**, 237 (1984); H. Aoki *et al.*, Phys. Rev. Lett. **54**, 831 (1985); J. T. Chalker *et al.*, Phys. Rev. Lett. **61**, 593 (1988); B. Huckestein *et al.*, Phys. Rev. Lett. **64**, 1437 (1990); Rev. Mod. Phys. **67**, 357 (1995); D. H. Lee *et al.*, Phys. Rev. Lett. **70**, 4130 (1993); B. Kramer *et al.*, Rep. Prog. Phys. **56**, 1469 (1993); T. Brandes *et al.*, Phys. Rev. Lett. **72**, 3582 (1994); S. R. E. Yang *et al.*, Phys. Rev. Lett. **74**, 3229 (1995); F. Evers *et al.*, Phys. Rev. B **64**, 241303(R) (2001).
[6] H. P. Wei *et al.*, Phys. Rev. Lett. **61**, 1294 (1988); S. Koch *et al.*, Phys. Rev. Lett. **67**, 883 (1991); L. W. Engel *et al.*, Phys. Rev. Lett. **71**, 2638 (1993); F. Kuchar *et al.*, Europhys. Lett. **49**, 480 (2000); F. Hohls *et al.*, Phys. Rev. Lett. **86**, 5124 (2001); **88**, 036802 (2002).
[7] M. Morgenstern *et al.*, Phys. Rev. Lett. **89**, 136806 (2002).
[8] M. Morgenstern *et al.*, J. Electron Spectrosc. Relat. Phenom. **109**, 127 (2000).
[9] S. Ilani (private communication).
[10] Chr. Wittneven *et al.*, Rev. Sci. Instrum. **68**, 3806 (1997).
[11] M. Morgenstern *et al.*, Phys. Rev. B **61**, 13805 (2000).
[12] LDOS and dI/dV coincide as long as V is small and electron-electron interactions are negligible; J. Tersoff *et al.*, Phys. Rev. Lett. **50**, 1998 (1983); Phys. Rev. B **31**, 805 (1985).
[13] R. Dombrowski *et al.*, Phys. Rev. B **59**, 8043 (1999).
[14] U. Merkt *et al.*, Phys. Rev. B **35**, 2460 (1987).
[15] L. Canali *et al.*, Appl. Phys. A **66**, S113 (1998).
[16] M. Morgenstern *et al.*, Phys. Rev. B **62**, 7257 (2000).
[17] T. Ando *et al.*, Rev. Mod. Phys. **54**, 437 (1982).
[18] E. I. Rashba *et al.*, Sov. Phys. Solid State **2**, 1109 (1960); D. Grundler, Phys. Rev. Lett. **84**, 6074 (2000).
[19] The disorder potential measured at $B = 0$ T and $B = 6$ T is nearly identical.
[20] The corrugation strength is defined as $(dI/dV_{\text{mean}} - dI/dV_{\text{min}})/dI/dV_{\text{mean}}$ with $dI/dV_{\text{mean(min)}}$ being the average (minimum) dI/dV value in an image.
[21] Chr. Wittneven *et al.*, Phys. Rev. Lett. **81**, 5616 (1998).
[22] D. Haude *et al.*, Phys. Rev. Lett. **86**, 1582 (2001); M. Morgenstern *et al.*, Phys. Rev. B **64**, 205104 (2001).
[23] To probe the extended state over an appropriate length scale, a temperature of about 50 mK is required.
[24] A. Chhabra *et al.*, Phys. Rev. Lett. **62**, 1327 (1989).
[25] The same analysis for the data of Ref. [22] show spectra which are a factor of 2 smaller in width.
[26] E. Schweitzer (private communication); for influences leading to a reduced α at the origin, see also T. Terao *et al.*, Phys. Rev. B **54**, 10 350 (1996).